This is a preprint, the final version is subject to change, of the American Mineralogist (MSA)
Cite as Authors (Year) Title. American Mineralogist, in press.
DOI: https://doi.org/10.2138/am-2019-7058

Revision 1

Change of crackling noise in granite by thermal damage: monitoring nuclear waste deposits

Kainan Xie, Xiang Jiang, Deyi Jiang, Yang Xiao, Shiwan Chen, Karin A. Dahmen, Eduard Vives, Antoni Planes, and Ekhard K.H. Salje

[1] State Key Laboratory of Coal Mine Disaster Dynamics and Control, Chongqing University, Chongqing 400044, P.R. China

[2] College of Civil Engineering, Chongqing University, Chongqing 400045, P.R. China

[3] Department of Earth Sciences, University of Cambridge, Cambridge CB2 3EQ, United Kingdom

[4] College of Resources and Environment Engineering, Guizhou University, Guiyang, 550025, P.R. China

[5] Department of Physics, University of Illinois at Urbana Champaign, Urbana, IL 61801, United States

[6] Departament de Física de la Matèria Condensada. Facultat de Física, Universitat de Barcelona. Martí i Franquès, 1, 08028 Barcelona, Catalonia.

[7] State Key Laboratory for Mechanical Behaviours of Materials, Xi'an Jiao Tong University, Xi'an 710049, P.R. China.

*Corresponding author: cqujiangxiang@163.com

This is a preprint, the final version is subject to change, of the American Mineralogist (MSA)
Cite as Authors (Year) Title. American Mineralogist, in press.
DOI: https://doi.org/10.2138/am-2019-7058

ABSTRACT

High-sensitivity detection of acoustic emission from granite under uniaxial stress, together with advanced statistical analysis, shows changing collapse mechanisms when a sample is pre-heated. Massive microstructural changes occur at temperatures > 500°C while low temperature (<<500°C) treatment leads to scale invariant crackling noise with a mixed fix-point behavior. After treatment at higher temperatures, the collapse occurs via acoustic signals that show energy distributions with systematic deviations from the Gutenberg-Richter law while the Omori's and Båth's laws are not influenced by the thermal treatment. The granite samples stem from the site in the Beishan mountains where a new burial site for nuclear waste will be constructed. According to the 13rd Five-Years Plan of the P.R. China, Chinese nuclear power installed capacity will reach 58 million kilowatts in 2020 and produce about 3200 tons of high-level nuclear waste every year. Monitoring the stability of the host rock at high temperatures becomes hence a key issue. Our analysis can serve as blueprint for a protocol for continuous monitoring of the burial site.

Keywords: crackling noise, granite, thermal damage; acoustic emission.

This is a preprint, the final version is subject to change, of the American Mineralogist (MSA)
Cite as Authors (Year) Title. American Mineralogist, in press.
DOI: https://doi.org/10.2138/am-2019-7058

INTRODUCTION

Mechanical and thermal damage of brittle matrix rocks is a key issue for nuclear waste disposal engineering. During the operation of a repository, the high-level radioactive waste will release heat continually. Constrained thermal expansion of the rock induces stresses, which modify the pre-existing stress field and could affect the long-term stability of a depository. The heat generated from high-level radioactive decay can aggravate rock stresses (Zhao et al. 2018). Additionally, new disposal way with very deep depth also associate with high temperature. Very deep disposal refers to boreholes drilled 4-5 km into the granitic basement. Radioactive decay gradually heats up the waste packages to a peak temperature (near 800 ◦C) to generate a substantial zone of partial melting in the granite surrounding the containers. As the heat output of the waste decreases, the melt slowly cools and recrystallizes to seal the packages into a sarcophagus of solid granite surrounded by zones of thermal metamorphism in which any pre-existing fractures are sealed by annealing and low-temperature hydration mineralization (Fergus and Philip 2013). Consequently, as discussed by a U.S. Geological Survey report (Bredehoeft et al. 1978), the thermal problem is an important factor in nuclear waste disposal. During the past three decades, many studies covered the mechanical behavior of rocks, few related to heating to high temperatures (Castillo-Villa et al. 2013; Salje and Dahmen 2014; Sethna et al. 2001; Soprunyuk et al. 2017). The Chinese development plan has foreseen to store nuclear waste in Beishan granite in the Gansu Province. This remote locality was chosen because of its

low permeability and high mechanical integrity. A key element for the suitability of this granite for the final deposition depends largely on its mechanical stability. A central issue is the uniaxial compressive strength, and elastic moduli of granite and its component minerals (Davidsen et al. 2007; Nataf et al. 2014a, 2014b). Furthermore, it is desirable to measure changes in the tectonic environment after the underground facilities are built. In this study we identify acoustic emission for the detection of crackling noise as a preferred, highly sensitive surveillance method.

Crackling noise as manifestation of mechanical avalanches is widely studied in porous materials and in natural earthquakes (Castillo-Villa et al. 2013; Sethna et al. 2001; Salje and Dahmen 2014; Soprunyuk et al. 2017). Critical distributions (power-law or double power-law) of energies, aftershocks and waiting times (Davidsen et al. 2007; Nataf et al. 2014a, 2014b; Ribeiro et al. 2015) have been reported from lab-quake experiments (Baró et al. 2013) in minerals and man-made materials (Castillo-Villa et al. 2013; Nataf et al. 2014a, 2014b; Salje et al. 2011, 2013; Soto-Parra et al. 2015) using the acoustic emission (AE) detection as experimental tool. AE activity typically increases near stress collapse (Byerlee 1978; Mansurov 1994;), confirmed by discrete element simulation of porous materials (Kun et al. 2013, 2014). In lab-quake experiments the superposition of several collapse mechanisms and hence combinations of avalanche characteristics were observed (Jiang et al. 2016, 2017; Salje et al. 2017). Typical examples are the compression of coal and sandstone with two power law exponents, the higher for randomly distributed bond-

breaking at the early compressive stage, and the smaller for densely correlated with collapse at a later stage. The crossover is a predictive criterion for imminent catastrophic collapse (Jiang et al. 2016, 2017). Other multiple collapse mechanisms occur in Ti-Ni shape memory alloys (Soto-Parra et al. 2015) where de-twinning and fracture are superposed. In this study, we show that the ratio between two collapse mechanisms, induced by thermal effects, characterizes the stability of Beishan granite.

EXPERIMENTAL METHODS

Beishan granite (BsG) specimens were first heated using the tube-furnace with a heating rate of 4°C /min to reach their test temperature (100°C, 200°C, 300°C, 400°C, 500°C, 600°C, and 700°C). The heating rate is sufficiently slow to avoid stress fractures due to thermal shock. The samples were then left at the anneal temperature for two hours; they were then cooled to room temperature inside the furnace. The cooling rate was ca. 1.67°C /min which is slow enough to avoid further micro cracking (Lin 2002). The effect of the high temperature treatment of the mineral grains and sample cracks were first observed by optical microscopy. Detailed low-field NMR analysis was then performed on BsG sample that were saturated with distilled water under 20 MPa for 12 h. These samples were placed in the NMR apparatus for testing their T_2 spectra, their porosity, permeability, and magnetic resonance imaging (MRI). Results of NMR and MRI results are collected in the supplementary material. In uniaxial compressive test, the stress rate was chosen to be $d\sigma/dt$= 8.5kPa/s (1kN/min) for all samples. AE signals were measured during compression

by two piezoelectric sensors (NANO-30 Physical Acoustics Company) fixed on the sample's round surface by rubber bands. The sensors were acoustically coupled to the sample by a thin layer of grease. The acoustic signal was pre-amplified (40 dB) and transferred to the AE analysis system (DISP from American Physical Acoustics Company, USA).

RESULTS

The energy distribution and super-jerks analysis

After anneal at different temperatures, the Beishan granite samples (more information about Beishan and Beishan granite in the supplementary material) were compressed and acoustic emission (AE) signals were measured (detailed AE experimental parameter setting in the supplementary materials). The probability distribution function P(E) of AE energies (aJ=10^{-18}J) was obtained by appropriate logarithmic binning of the AE signals. Figure 1a shows P(E) in log-log plots for BsG samples with thermal damage for anneal at 100, 200, 300, 400, 500, 600, and 700°C. At first glance, rather good power law distributions $P(E) \sim E^{-\varepsilon}$ are observed over more than eight decades for low temperature treatments and seven decades for high temperature treatments. The distributions for 100°C to 500°C are very similar with the slope ε increasing (becoming more negative) for 600°C and 700°C. To investigate the variation of these distributions in more detail, we apply the Maximum Likelihood (ML) method (Clauset 2009) that consists in fitting the exponent as a function of a running minimum energy cutoff E_{min}. When the fitted exponent shows a well-defined

plateau with E_{min}, one can conclude about a good power-law behavior with a true exponent ε. Results corresponding to the present data are shown in Figure 1b. For low annealing temperatures (below 600 ºC) we find a maximum reaching $\varepsilon \approx 1.6 \pm 0.1$ followed by a minimum with $\varepsilon \approx 1.3$ - 1.4. No plateaus but a continuous increase of the ML curve occurs for higher temperatures. (above 600 ºC)

These ML-shapes reflect whether the recorded data set corresponds to a unique crackling noise mechanism, whether it is distorted by exponential damping factors or it corresponds to a mixture of several crackling noise mechanisms (Salje et al. 2017). Similar mixing effects were seen previously in compressed coal samples (Jiang et al, 2016, 2017; Xu et al. 2019). Increasing ML-curves are characteristic for damping effects, while the ML-curve at low temperatures are typical for mixing of two power laws. Figure 1c shows the energy distribution corresponding to the sample heat treated at 700°C and the corresponding fit to a power function with damping. $P(E) \sim E^{-\varepsilon} \exp(-CE)$, with $\varepsilon = 1.75$ and $C = 10^{-6}$ aJ^{-1} This value of the exponent should be understood, not as a true critical exponent, but instead as an effective exponent.

To examine the relation between ML signatures and the failure process, we studied the ML behavior in different time stages and reduced the AE spectrum from the whole set to subsets of super-jerks (Jiang et al. 2017). A super-jerk is defined as an avalanche signals with energy greater than any previous event of the series (figure2a, 2b). They are numbered by

their rank k=1,2…, and divide the full event series into small subsets (Davidsen et al. 2006, 2008; Jiang et al. 2017; Pál et al. 2016; Soprunyuk et al. 2017; Wergen and Krug 2010; Yoder et al. 2010). The super-jerk analysis is shown in figure 2c ,2d for data at 100 ◦C and 700 C respectively, with ML curves for all subsets as a function of rank k.

The behavior of the ML-curves for interjerk subsets confirms that the mixture of exponents found for samples treated at low T (figure 2e), is a consequence of the fact that the critical exponent changes in time from a high value close to 1.65, to a lower value close to 1.4 for subsets corresponding to the latest superjerks. The failure mechanism at 700◦C (figure 2d) is very different: the exponents corresponding to interjerk subsets do not decrease with increasing rank (figure2d, 2f). All data are highly damped with an effective exponent uniformly near 1.75. A better description of the behavior of the exponents with superjerk rank k, can be obtained by averaging the curves in 2d and 2e from 10^1 aJ to 10^4 aJ. The results are shown in figures 2e and 2f.

Decreasing exponents under stress (100◦C) (figure 2e) are commonly observed for changeovers from randomly distributed bond-breaking to highly correlated collapse along shear zones (see Fig 2g) (Jiang et al. 2016; Kun et al. 2013, 2014). In the granite sample 700◦C, no obvious shear zones occur while much clastic material is generated (figure2h). The sample ‘crumbles’. The differences for the formation of cracks by thermal treatment cracks becomes obvious when observed by optical microscope (see supplementary materials) and NMR. Figure.3a-3f show the proton density weighted images of horizontal

cross-section. We find that proton densities are distributed homogenously when the annealing temperature is below 500°C. No significant clustering of proton densities was observed. The cluster of high density of ^{1}H is induced by interaction and coalescence of larger micro-cracks. When the annealing temperature increases to 600°C and 700 °C, cluster of high density of ^{1}H are observed.

Local collapse is attributed to the motion of cracks and interfaces. They occur either randomly (Gaussian size distribution) or they obey a power-law-type size distribution, indicating self-organized criticality (Falk and Langer 1998; Zink et al. 2006). In our granite sample, only the latter scenario was observed, which indicate some long-range strain interactions between the collapse events. Collective plastic events, like 'shear transformation zones' (STZs) (Falk and Langer 1998), require the localization of stress relaxations in ensembles of about 100 atoms (Eshelby 1957; Picard et al. 2005). In mean field descriptions of viscoplasticity (Falk and Langer 1998) STZs are often regarded to act independently although they indeed carry long-range elastic stress fields causing cooperative effects (Martens et al. 2012; Neudecker and Mayr 2009). Their collective activation is responsible for the emergence of macroscopic shear bands (Karmakar et al. 2010), and hence plasticity. Such shear bands are observed for low temperature anneal but not at high temperatures where the clastic collapse dominates. This effect is mirrored in the damping during AE: damping is low during the classic viscoplastic collapse at low

annealing temperatures but very high when the sample disintegrates into small clastic grains at high temperatures.

The waiting time distribution

A 'waiting time' is the time interval between two subsequent avalanches, seen as two AE jerks. Figure 4 shows the distribution of waiting times for samples with thermal damage for annealing at different temperatures. The inset figure shows the waiting time distribution after normalization by its average. After normalization, all our waiting time distributions collapse into a single double power law (Baró et al. 2013; Corral 2003). The two exponents for the waiting time distribution (1.4 for small segment and 2.5 for large segment) agree with the results of other natural or artificial SiO_2 based materials (Nataf et al. 2014a). Unlike the energy distribution, the temporal character was little affected by the annealing. The temporal distribution often shows robustness in earthquake analysis, the distribution holds from worldwide to local scales for quite different tectonic environments. This is even true if the seismic rate is not stationary as during periods of pronounced aftershock sequences (Bak et al. 2002; Davidsen et al. 2007).

Omori's and Båth's law

Omori's law (Utsu et al. 1995) describes the statistical behavior of aftershocks (AS). An aftershock is a smaller signal that occurs after a previous large shock. If an aftershock is

larger than the main shock, the AS sequence is finished and the new large aftershock is re-designated as a new main shock. Omori's law states that the number of AS decays as a power-law after each mainshock (MS). We define MS as AE signals with energies E_{MS} between 10^i to 10^{i+1} aJ, with i = 1, 2, and 3. Figure 5 shows the results of 100°C and 700°C for different E_{MS}. The power law dependence is emphasized by the averaged slope with Omori exponents p=0.9. Omori's law distributions of 100°C and 700°C do not show obvious differences.

Båth's law (Båth 1965; Console et al. 2003) states that the average ratio of the energy magnitudes of one MS and its AS* (the largest aftershock) is about 1.2. The ratio or 'relative magnitude' is defined as $<\Delta M>=\log(E_{MS}/E_{AS*})$. Figure 6 shows the relative magnitude as a function of mainshock energy $E_{MS} > 10^2$ aJ. The result agrees well with Båth's law. The convergence can be well described by an extended Debye model (Jiang et al.2016) with an upper limit for $<\Delta M> = 1.18$. We also find that the curves show a slight trend to decrease for large values of E_{MS}. A simulation study using the ETAS model showed the same tendency for the relative magnitude controlled by the parameter α in the ETAS model (Helmstetter and Sornette 2003). When α=1, our results show excellent consistency with simulations. There is no significant difference for samples with different annealing temperatures.

This is a preprint, the final version is subject to change, of the American Mineralogist (MSA)
Cite as Authors (Year) Title. American Mineralogist, in press.
DOI: https://doi.org/10.2138/am-2019-7058

DISCUSSION

Beishan granite is sensitive to thermal treatment. The main effect stems from the formation of cracks during high temperature anneal. Microscopic and NMR analysis show that the micro structure of granite changes dramatically near the transition temperature in quartz (supplementary materials) with intense crack formation at higher temperatures. The AE reflects these changes. After treatments at low temperatures a superposition of two power laws with different exponents dominates. This crossover behavior is consistent with previous results in coal, sandstone (Jiang et al. 2016), and Ti-Ni alloy (Soto-Parra et al. 2015). Discrete element simulations (Kun et al. 2013, 2014), including fiber bundle and electrical fuse model (Pradhan et al. 2005), result in similar multiple-fix point behavior.

At high temperatures, we find no indication of power law mixing but observe very high damping of a single power law with a high effective exponent (ε=1.75). The main thermal damage trigger mechanism may be that the differential thermal expansion between quartz and feldspar leads to cracks both at interfaces and inside quartz (Carpenter et al. 1998; Kranz 1983). From a microscopic perspective, thermal cracking in granite occurs via two different mechanisms (Chen et al. 2017; Fredrich and Wong 1986; Jansen et al.1993; Richter and Simmons 1974; Wang et al. 1989). First, mismatch and anisotropy in thermal expansion coefficients between adjacent crystalline grains in a homogeneous temperature field result in sufficiently high stresses for the formation of thermal cycling cracks when the temperature exceeds a threshold. Second, thermal gradient cracks can also be generated

when thermal stresses, due to an inhomogeneous temperature field, exceed the local tensile strength of the rock. The temperature range covers two important perturbations in quartz. First, there is an extrinsic effect of cracking around multiple microscopic bubbles filled with liquid/vapor mixtures, which are usually contained in quartz and quartz-containing rocks (Godbeer and Wilkins 1967; Hall and Bodnar 1989). At temperatures higher than the homogenization point in aqueous inclusions (310°C), the internal pressure in bubbles reduces significantly the material strength (Kendrick et al. 2006). This process is consistent with figure 3c, which shows the proton density begins to increase. With increasing temperature, a 1.7% increase in the crystal volume at 573 °C at the phase transition $\alpha \rightarrow \beta$ of quartz causes further crumbling. Glover et al. (1995) studied thermal damage in different rock types by monitored using acoustic emissions. The peak of AE hit rate is coincident with the α/β phase transition in quartz (573°C). Reuschle´ (1989) has shown that the surface energy of quartz becomes low at the α/β phase transition, and little energy is dissipated per unit length of new crack formation. Many new cracks need to be formed to enable the rock matrix to dissipate the deformation energy accumulated as stresses in the minerals. Above 600°C, X-ray showed trans-granular crack generates across the biotite with high density, and the boundary crack and trans-granular crack propagates and coalesces throughout the entire granite (Fan et al.2018). These results agree with our study.

A simple analytic theory for the statistics of avalanches in sheared granular materials may relate to deviations from the fixed-point (Dahmen et al. 2011). In this theory, avalanche

size distribution will change from pure power to damping power when decreasing granular fraction. Granular fraction is proportion to the rescaled packing fraction. The result of analytically predicted mean field slip avalanche size distribution D(s) for decreasing granular number fractions is similar to figure1a in this paper.

IMPLICATION

The results of our research have two major implications. Firstly, it can be used for continuous monitoring of the burial site and other geothermal engineering. The AE energy distribution exponent can easily be measured using highly sensitive AE sensors attached to the host rock or normal sensors located around the burial site. The data analysis method used in this study also can be easily implemented through online evaluation of the AE signals. In principle, the statistical results obtained in small samples can be scaled from lab to field-scale (Baró et al. 2013, Nataf et al. 2014). Recently, by comparing coal and charcoal samples under compression with real earthquake data it has been confirmed that the scaling improves when the samples are more heterogeneous and the mechanisms giving rise to AE are dominated by friction effects between grains (Xu et al 2019). However, the laboratory results should always be taken with caution and extensive testing is needed in order to determine the true forecasting power of this approach and to which extent it could provide guidance for policies and operational decisions.

In addition, the relationship between mineral structure and avalanche dynamics is the focus

of many studies of crackling noise. Here we show that avalanches are heavily influenced by temperature and that local 'crumbling' is a key mechanism for softening of geomaterials (rather than elastic softening). This result will now attract more theoretical and simulation studies in this field.

ACKNOWLEDGEMENTS

K. Xie, D. Jiang and X. Jiang acknowledge financial support from the National Science and Technology Major Project (Grant No.2016ZX05045001-005), and graduate research and innovation foundation of Chongqing (CYB18031). E.K.H. Salje is grateful to EPSRC (EP/P024904/1) for support. E.Vives and A.Planes acknowledge financial support from CICyT (Spain) project MAT2016-75823-R.

REFERENCES CITED

Bak, P., Christensen, K., Danon, L., and Scanlon T. (2002) Unified Scaling Law for Earthquakes. Physical Review Letters, 88, 178501.

Baró, J., Corral, A., Illa, X., Planes, A., Salje, E.K.H., Schranz, W., Soto-Parra, D.E., and Vives, E. (2013) Statistical similarity between the compression of a porous material and earthquakes. Physical Review Letters, 110, 088702.

Båth, M. (1965) Lateral inhomogeneities of the upper mantle. Tectonophysics, 2, 483-514.

Bredehoeft, J.D., England, A.W., Stewart, D.B., Trask, N.J., and Winograd, I.J. (1978) Geologic disposal of high-level radioactive wastes-earth science perspectives. Dept. of Interior, Geological Survey Circular, No. 779.

Byerlee, J., (1978) A review of rock mechanics studies in the United States pertinent to earthquake prediction. Pure and Applied Geophysics, 116, 586-602.

Carpenter, M.A., Salje, E.K.H., Graeme-Barber, A., Wruck, B., Dove, M.T., and Knight, K.S. (1998) Calibration of excess thermodynamic properties and elastic constant variations associated with the alpha-beta phase transition in quartz. American Mineralogist, 83, 2-22.

Castillo-Villa, P.O., Baró, J., Planes, A., Salje, E.H.K., Sellappan, P., Kriven, W.M., and Vives, E. (2013) Crackling noise during failure of alumina under compression: The effect of porosity. Journal of Physics: Condensed Matter, 25, 292202.

Chen, S., Yang, C., and Wang, G. (2017) Evolution of thermal damage and permeability of Beishan granite. Applied Thermal Engineering, 110,1533–1542.

Clauset, A., Shalizi, C.R., and Newman, M.E. (2009) Power-law distributions in empirical

data. Society for Industrial and Applied Mathematics Review, 51, 661-703.

Console, R., Lombardi, A.M., Murru, M., and Rhoades, D. (2003) Båth's law and the self-similarity of earthquakes. Journal of Geophysical Research: Solid Earth, 108, B22128.

Corral, A´., (2003) Local distributions and rate fluctuations in a unified scaling law for earthquakes. Physical Review E, 68, 035102(R).

Dahmen, K.A., Ben-Zion, Y. and Uhl, J T. (2011) A simple analytic theory for the statistics of avalanches in sheared granular materials. Nature Physics, 7, 554–557.

Davidsen, J., Grassberger, P., and Paczuski, M. (2006) Earthquake recurrence as a record breaking process. Geophysical Research Letters, 33, l11304.

Davidsen, J., Stanchits, S., and Dresen, G. (2007) Scaling and universality in rock fracture. Physical Review Letters, 98, 125502.

Davidsen, J., Grassberger, P., and Paczuski, M. (2008) Networks of recurrent events, a theory of records, and an application to finding causal signatures in seismicity. Physical Review E, 77, 066104.

Eshelby, J. D. (1957) The determination of the elastic field of an ellipsoidal inclusion, and related problems. Proceedings of the Royal Society A, 241, 376–396.

Falk, M.L., and Langer, J.S. (1998) Dynamics of viscoplastic deformation in amorphous solids. Physical Review E, 57, 7192–7205.

Fan, L.F., Gao, J.W., Wu, Z.J., Yang, S.Q., Ma, G.W. (2018) An investigation of thermal effects on micro-properties of granite by X-ray CT technique. Applied Thermal Engineering, 140, 505–519.

Fergus, G.F.G, and Philip G. A. (2003) Granite recrystallization: The key to the nuclear waste problem? Geology, 31, 657-660.

Fredrich, J.T., and Wong, T.F. (1986) Micromechanics of thermally induced cracking in three crustal rocks. Journal of Geophysical Research 91,12743–12764.

Glover, P.W.J., Baud, P., Darot, M., Meredith, P.G., Boon, S.A., LeRavaleq, M., Zoussi, S., and Reusche, T. (1995) α/β phase transition in quartz monitored using acoustic emissions. Geophysical Journal International, 120, 775-782.

Godbeer, W.C., and Wilkins, R.W.T. (1967) The water content of a synthetic quartz. American Mineralogist, 62, 831–832.

Hall, L., and Bodnar, R.J. (1989) Comparison of fluid inclusion decrepitation and acoustic emission profiles of Westerly granites and quartzite. Tectonophysics, 168, 283–296.

Helmstetter, A., and Sornette, D. (2003) Båth's law Derived from the Gutenberg-Richter law and from Aftershock Properties. Geophysical Research Letters, 30, 20,2069.

Jansen, D.P., Carlson, S.R., Young, R.P., and Hutchins, D.A. (1993) Ultra-sonic imaging and acoustic emission monitoring of thermally induced microcracks in Lacdu Bonnet granite. Journal of Geophysical Research, 98,22231–22243.

Jiang, X., Jiang, D., Chen, J., and Salje, E.K.H. (2016) Collapsing minerals: Crackling noise of sandstone and coal, and the predictability of mining accidents. American Mineralogist, 101, 2751-2758.

Jiang, X., Liu, H., Main, I.G., and Salje, E.K.H. (2017) Predicting mining collapse: Superjerks and the appearance of record-breaking events in coal as collapse precursors. Physical Review E, 96, 023004.

Karmakar, S., Lerner, E., Procaccia, I., and Zylberg, J. (2010) Statistical physics of elastoplastic steady states in amorphous solids: finite temperatures and strain rates. Physical Review E, 82, 031301.

Kendrick, M.A., Phillips, D., Miller, J.M., (2006) Part I. Decrepitation and degassing behaviour of quartz up to 1560 °C: analysis of noble gases and halogens in complex fluid inclusion assemblages. Geochimica et Cosmochimica Acta, 70, 2540–2561.

Kranz, R.L. (1983) Microcracks in rocks: a review. Tectonophysics, 100, 449–480.

Kun, F., Varga, I., Lennartz-Sassinek, S., and Main, I.G. (2013) Approach to failure in porous granular materials under compression. Physical Review E, 88, 062207.

Kun, F., Varga, I., Lennartz-Sassinek, S., and Main, I.G. (2014) Rupture cascades in a discrete element model of a porous sedimentary rock. Physical Review Letters, 112, 065501.

Lin W. (2002) Permanent strain of thermal expansion and thermally induced microcracking in Inada granite. Journal of Geophysical Research-atmospheres, 107, 3-16.

Mansurov V.A. (1994) Acoustic emission from failing rock behavior. Rock Mechanics and

Rock Engineering, 27, 173-182.

Martens, K., Bocquet, L., and Barrat, J.L. (2012). Spontaneous formation of permanent shear bands in a mesoscopic model of flowing disordered matter. Soft Matter, 8, 4197–4205.

Nataf, G.F., Castillo-Villa, P.O., Baró, J., Illa, X., Vives, E., Planes, A., and Salje, E.K.H. (2014a) Avalanches in compressed porous SiO2-based materials. Physical Review E, 90, 022405.

Nataf, G.F., Castillo-Villa, P.O., Sellappan, P., Kriven, W.M., Vives, E., Planes, A., and Salje, E.K.H. (2014b) Predicting failure: acoustic emission of berlinite under compression. Journal of Physics: Condensed Matter, 26, 275401.

Neudecker, M., and Mayr, S.G. (2009) Dynamics of shear localization and stress relaxation in amorphous. Acta Materialia, 57, 1437–1441.

Pál, G., Raischel, F., Lennartz-Sassinek, S., Kun, F., and Main, I. G. (2016) Record-breaking events during the compressive failure of porous materials. Physical Review E, 93, 033006.

Picard, G., Ajdari, A., Lequeux, F.M.C., and Bocquet, L. (2005) Slow flows of yield stress fluids: complex spatiotemporal behaviour within a simple elastoplastic model. Physical Review E, 71, 010501.

Pradhan, S., Hansen, A., and Hemmer, P.C. (2005) Crossover behavior in burst avalanches: Signature of imminent failure. Physical Review Letters, 95, 125501.

Ribeiro, H.V., Costa, L.S., Alves, L.G.A., Santoro, P.A., Picoli, S., Lenzi, E.K., and Mendes, R.S. (2015) Analogies between the cracking noise of ethanol-dampened charcoal and earthquakes. Physical Review Letters, 115, 025503.

Richter, D. and Simmons, G. (1974) Thermal expansion behavior of igneous rocks. International Journal of Rock Mechanics and Mining Science 11,403–411.

Reuschle´, T., (1989) Les fluides et I'evolution des proprieties, mechaniques des roches, PhD Thesis, Louis Pasteur University, Strasbourg.

Salje, E.K.H., Soto-Parra, D.E, Planes, A., Vives, E., Reineckerc, M., and Schranz, W. (2011) Failure mechanism in porous materials under compression: Crackling noise in mesoporous SiO_2. Philosophical Magazine Letters, 91, 554-560.

Salje, E.K.H., Lampronti, G.I., Soto-Parra, D.E., Baro´ J., Planes, A., and Vives, E. (2013) Noise of collapsing minerals: Predictability of the compressional failure in goethite mines. American Mineralogist, 98, 609-615.

Salje, E.K.H., and Dahmen, K.A. (2014) Crackling noise in disordered materials. Annual Review of Condensed Matter Physics, 5, 233-254.

Salje, E.K.H., Planes A., and Vives, E. (2017) Analysis of crackling noise using the maximum-likelihood method: Power-law mixing and exponential damping. Physical Review E, 96, 042122.

Sethna, J.P., Dahmen, K.A., and Myers, C.R. (2001) Crackling noise. Nature, 410, 242-250.

Soprunyuk, V., Puchberger, S., Tröster, A., Vives, E., Salje, E.K.H., and Schranz, W. (2017) Strain intermittency due to avalanches in ferroelastic and porous materials Journal of Physics: Condensed Matter, 29, 224002.

Soto-Parra, D., Zhang X., Cao S., Vives E., Salje E.K.H., and Planes A. (2015) Avalanches in compressed Ti-Ni shape-memory porous alloys: An acoustic emission study. Physical

Review E, 91, 060401.

Xu, Y., Angeles G. B., Planes, A., Ding, X., and Vives, E. (2019) Criticality in failure under compression: acoustic emission study of coal and charcoal with different microstructures. Physical Review E, 99, 033001

Utsu, T., Ogata, Y., and Matsu'ura, R.S. (1995) The centenary of the omori formula for a decay law of aftershock activity. Journal of Physics of the Earth, 43, 1-33.

Wang, H.F., Bonner, B.P., Carlson, S.R., Kowallis, B.J., and Heard, H.C. (1989) Thermal stress cracking in granite. Journal of Geophysical Research, 94, 1745–1758.

Wergen, G., and Krug, J. (2010) Record-breaking temperatures reveal a warming climate. Europhysics Letters, 92, 30008.

Yoder, M. R., Turcotte, D. L., and Rundle, J. B. (2010) Record-breaking earthquake intervals in a global catalogue and an aftershock sequence. Nonlinear Processes in Geophysics, 17, 169-176.

Zhao, X.G., Zhao, Z., Guo, Z., Cai, M., Li, X., Li, P.F., Chen, L., and Wang, J. (2018) Influence of Thermal Treatment on the Thermal Conductivity of Beishan Granite.

Rock Mechanics and Rock Engineering, 51, 2055–2074.

Zink, M., Samwer, K., Johnson, W.L., and Mayr, S.G. (2006) Plastic deformation of metallic glasses: size of shear transformation zones from molecular dynamics simulations. Physical Review B, 73, 172203.

This is a preprint, the final version is subject to change, of the American Mineralogist (MSA)
Cite as Authors (Year) Title. American Mineralogist, in press.
DOI: https://doi.org/10.2138/am-2019-7058

FIGURES

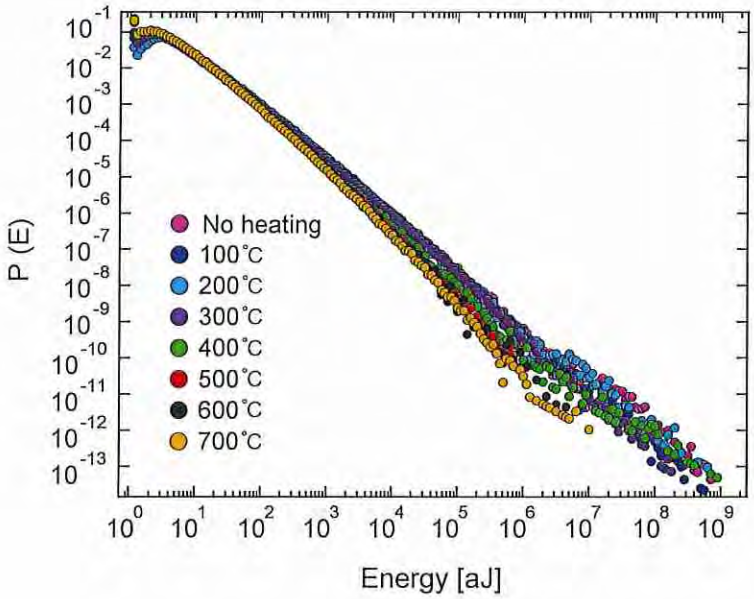

(a)

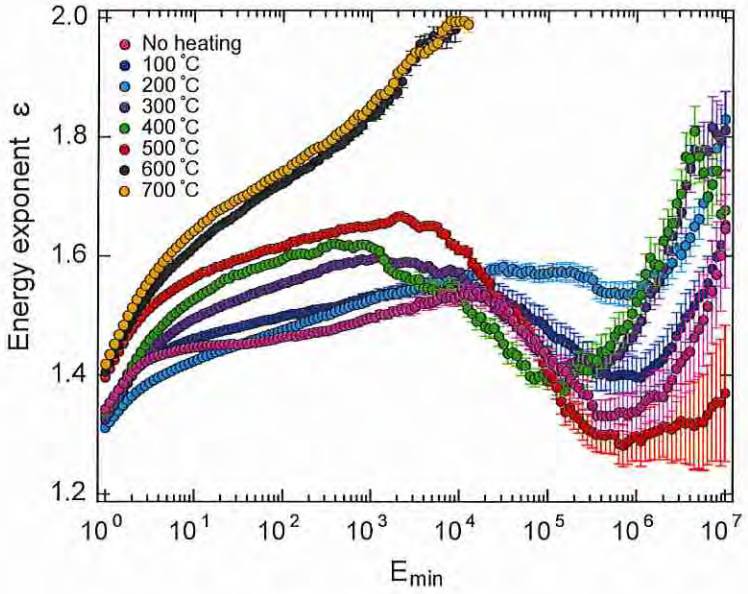

(b)

This is a preprint, the final version is subject to change, of the American Mineralogist (MSA)
Cite as Authors (Year) Title. American Mineralogist, in press.
DOI: https://doi.org/10.2138/am-2019-7058

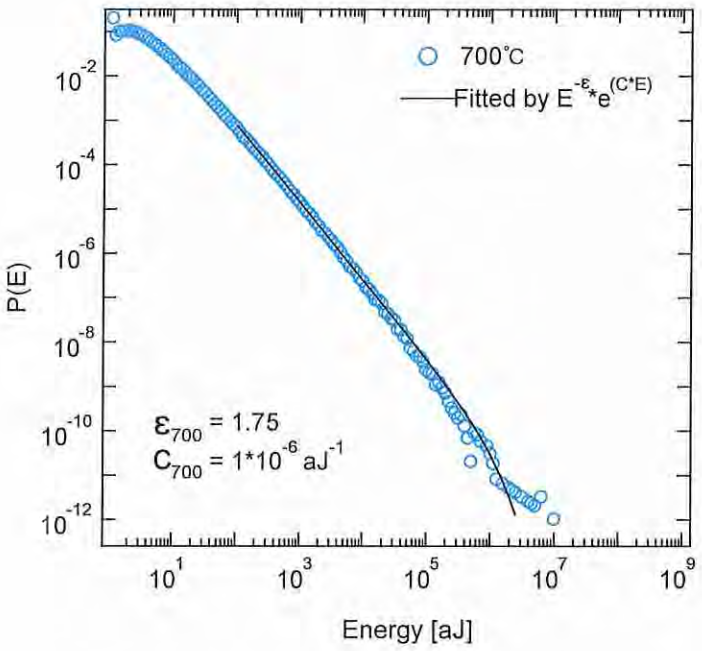

(c)

Figure 1. (a) Distribution of avalanche absolute energies for different temperatures. (b) The ML-fitting exponent ε as a function of a lower threshold E_{min}. Typical error bars are indicated (c) Fitting of a damped power-law to the distribution of avalanche energies after heat treatment at 700°C..

This is a preprint, the final version is subject to change, of the American Mineralogist (MSA)
Cite as Authors (Year) Title. American Mineralogist, in press.
DOI: https://doi.org/10.2138/am-2019-7058

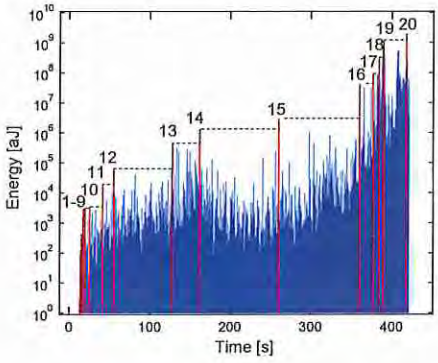

(a)

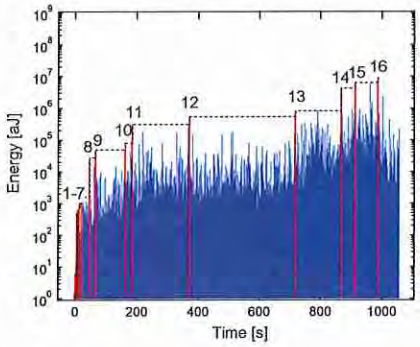

(b)

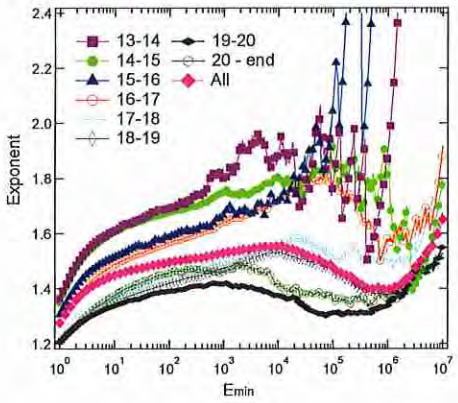

(c)

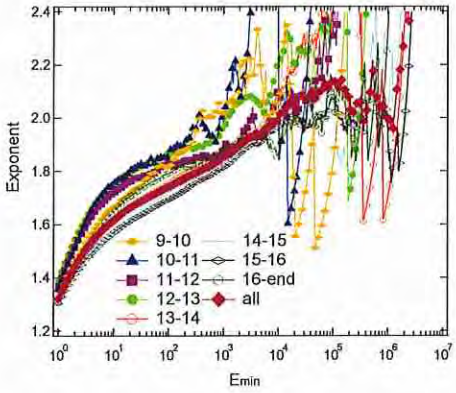

(d)

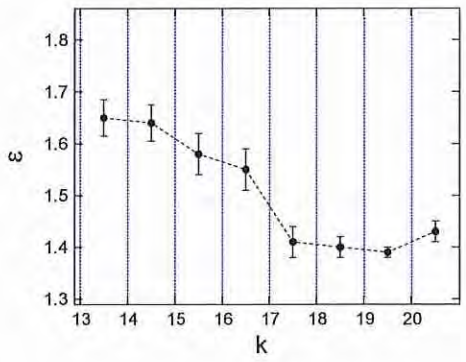

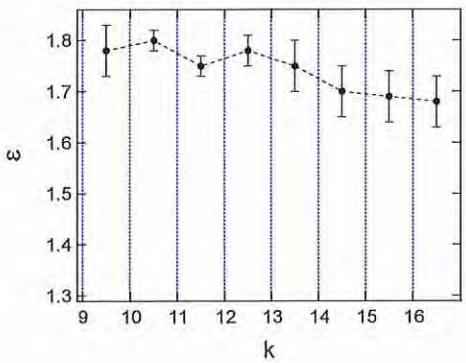

This is a preprint, the final version is subject to change, of the American Mineralogist (MSA)
Cite as Authors (Year) Title. American Mineralogist, in press.
DOI: https://doi.org/10.2138/am-2019-7058

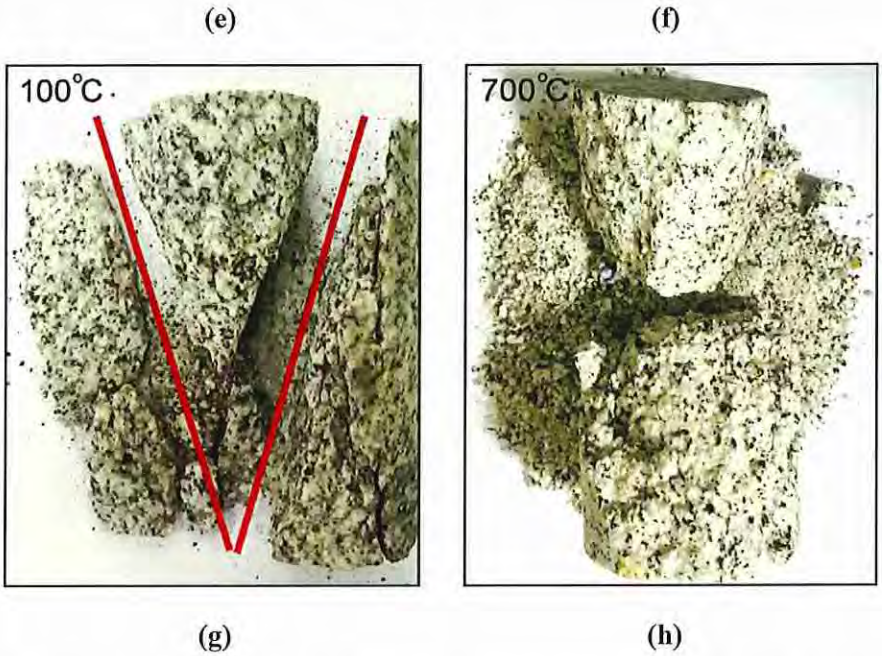

Figure 2. (a)(100°C) and (b)(700°C) are the time sequence of AE events in granite under uniaxial compression. Red signals are super-jerks which are more energetic than any of the previous signals. (c) (100°C) and (d) (700°C) are the ML curves with energy exponent as a function of the lower energy cutoff for different super-jerk ranks. (e) (100°C) and (f) (700°C) are the relation between the effective energy exponent ε and the loading (indicated by super-jerk ranks). (g)(100°C) and (h)(700°C) are the photographs of granite samples after collapse, red lines show the obvious shear failure face.

This is a preprint, the final version is subject to change, of the American Mineralogist (MSA)
Cite as Authors (Year) Title. American Mineralogist, in press.
DOI: https://doi.org/10.2138/am-2019-7058

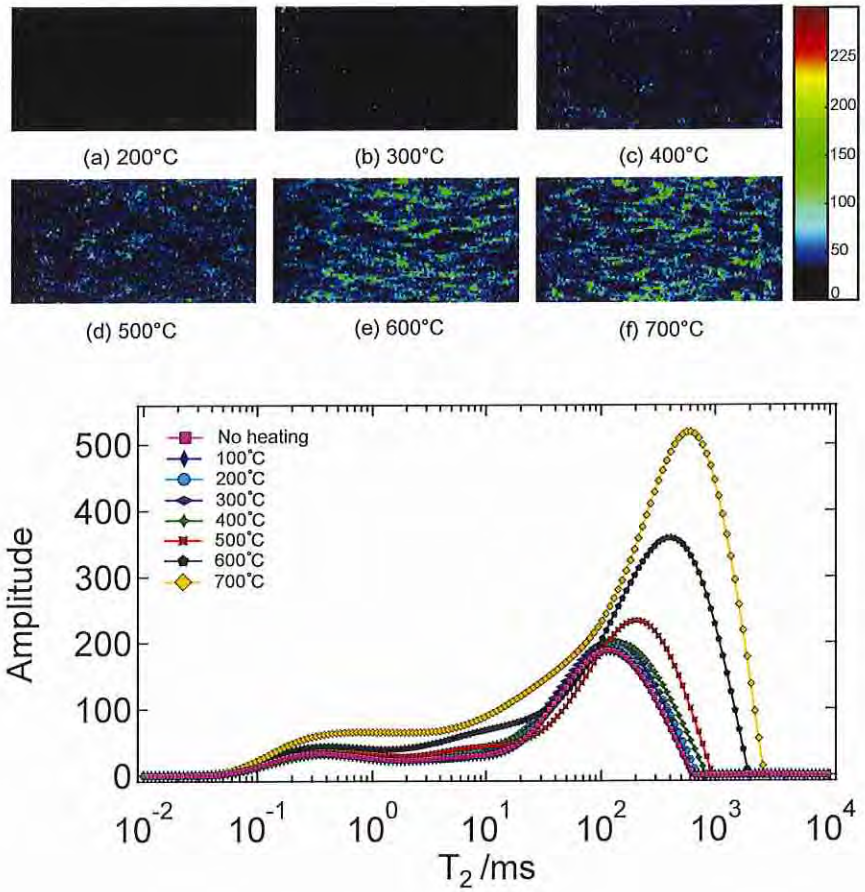

(g)

Figure.3. (a)-(f) Proton density weighted images of cross-section for samples treated by different temperatures. Water enters into cracks, the images show high proton density with strong MRI signals amplitude. The color bar provides a relative scale for the moisture content. (g) NMR T_2 relaxation time for BsG samples after anneal at different temperatures.

This is a preprint, the final version is subject to change, of the American Mineralogist (MSA)
Cite as Authors (Year) Title. American Mineralogist, in press.
DOI: https://doi.org/10.2138/am-2019-7058

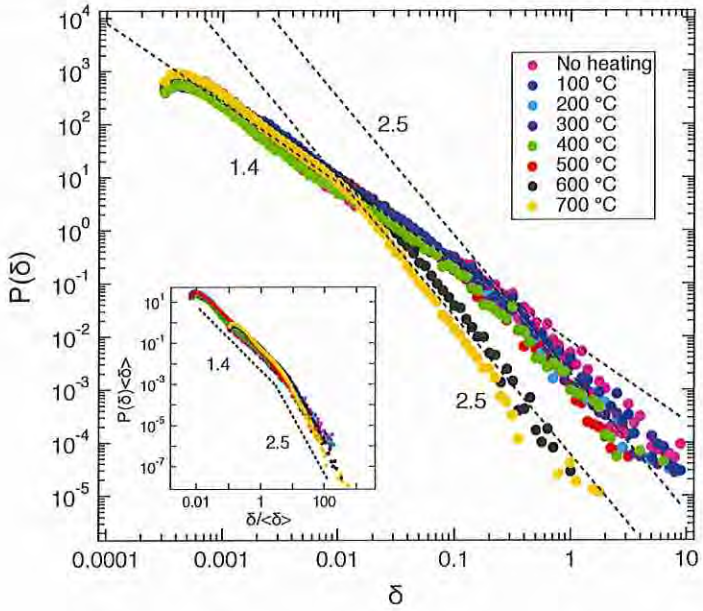

Figure 4. Histogram distributions of waiting times for granite samples annealed at different temperatures. The insert figure shows the waiting time distribution after normalized by its average <δ>.

This is a preprint, the final version is subject to change, of the American Mineralogist (MSA)
Cite as Authors (Year) Title. American Mineralogist, in press.
DOI: https://doi.org/10.2138/am-2019-7058

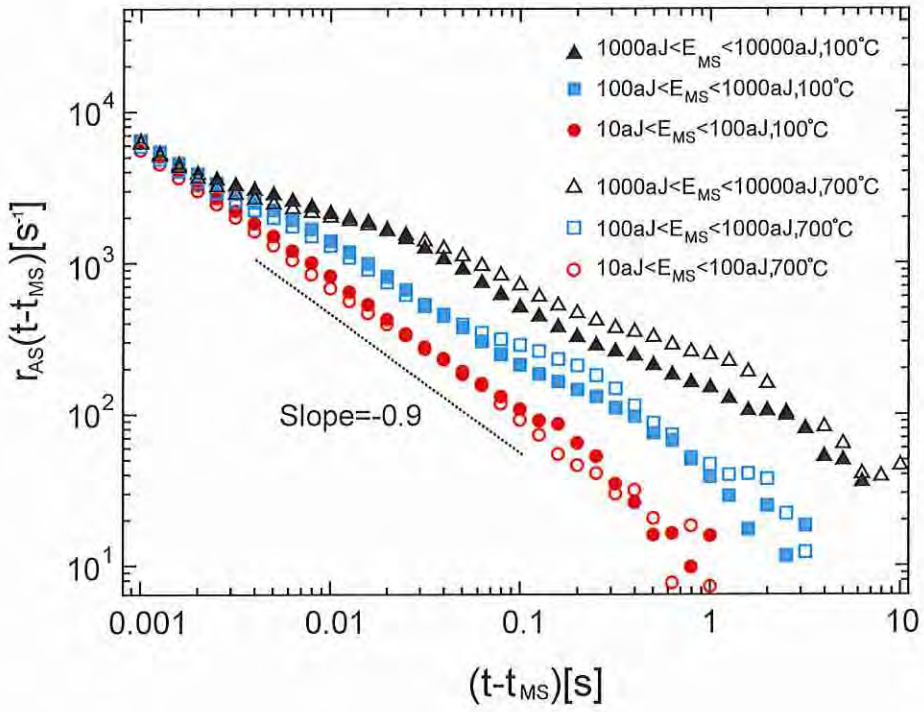

Figure 5. Rate of aftershocks per unit time, r, as a function of the time lapse to the main shock for 100°C and 700°C.

This is a preprint, the final version is subject to change, of the American Mineralogist (MSA)
Cite as Authors (Year) Title. American Mineralogist, in press.
DOI: https://doi.org/10.2138/am-2019-7058

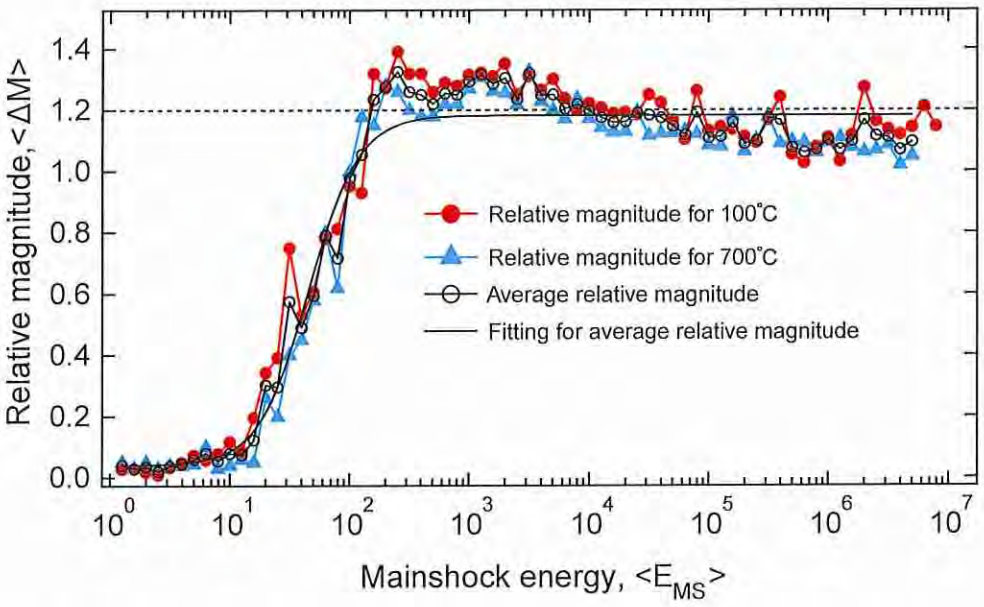

Figure 6. The relationship between relative magnitude and mainshock energy for 100°C, 700°C, and its average. Solid black line is a fit to an extended Debye model with an upper limit 1.18. Dashed horizontal line (1.2) indicates the relative magnitude from Båth's law.